Journal of ELECTRONIC MATERIALS, Vol. 49, No. 1, 2020
https://doi.org/10.1007/s11664-019-07454-6

Interplay of Wettability, Interfacial Reaction and Interfacial Thermal Conductance in Sn-0.7Cu Solder Alloy/Substrate Couples

THIAGO SOARES,[1] CLARISSA CRUZ,[1] BISMARCK SILVA,[2] CRYSTOPHER BRITO,[3] AMAURI GARCIA,[1] JOSÉ EDUARDO SPINELLI ,[4,5] and NOÉ CHEUNG[1]

1.—Department of Manufacturing and Materials Engineering, University of Campinas UNICAMP, Campinas, SP 13083-860, Brazil. 2.—Department of Materials Engineering, Federal University of Rio Grande do Norte-UFRN, Natal 59078-970, Brazil. 3.—Campus of São João da Boa Vista, São Paulo State University - UNESP, São João da Boa Vista, SP 13876-750, Brazil. 4.—Department of Materials Engineering, Federal University of São Carlos, UFSCar, São Carlos, SP 13565-905, Brazil. 5.—e-mail: spinelli@ufscar.br

Directional solidification experiments coupled with mathematical modelling, drop shape analyses and evaluation of the reaction layers were performed for three different types of joints produced with the Sn-0.7 wt.%Cu solder alloy. The association of such findings allowed understanding the mechanisms affecting the heat transfer efficiency between this alloy and substrates of interest. Nickel (Ni) and copper (Cu) were tested since they are considered work piece materials of importance in electronic soldering. Moreover, low carbon steel was tested as a matter of comparison. For each tested case, wetting angles, integrity and nature of the interfaces and transient heat transfer coefficients, '*h*', were determined. Even though the copper has a thermal conductivity greater than nickel, it is demonstrated that the occurrence of voids at the copper interface during alloy soldering may decrease the heat transfer efficiency, i.e., '*h*'. Oppositely, a more stable and less defective reaction layer was formed for the alloy/nickel couple. This is due to the suppression of the undesirable thermal contraction since the hexagonal Cu_6Sn_5 intermetallics is stable at temperatures below 186°C in the presence of nickel.

Key words: Sn-Cu alloy, solders, reaction layer, heat transfer, wettability, solidification

INTRODUCTION

Over the past decades, eutectic or near eutectic alloys of the Sn-Pb system have been extensively used in soldering processes. Bearing in mind that lead is a toxic metal, its use has been reduced through environmental directives such as the Restriction of Hazardous Substances (RoHS) of the European Union,[1] firstly applied in 2011. Concession for the use of lead has been allowed for automotive parts until 2023.[2,3]

Thus, the need for new non-toxic alloys for applications in the electronics industry is a critical and urgent task to meet the current demand for microelectronic assembly. In this context, lead-free solder alloys (LFSA)[4] become alternatives to the replacement of Sn-Pb solder alloys as joining material. Among several lead-free solders, a series of Sn-Cu alloys have emerged as the most commonly accepted. It is mainly mentioned in eutectic or near-eutectic compositions from 0.7 wt.%Cu to 0.9 wt.%Cu.[5–7] The eutectic Sn-0.7 wt.%Cu alloy melts at 227°C. The Sn-Cu alloys may be employed

(Received March 28, 2019; accepted July 17, 2019; published online July 31, 2019)

for medium temperature soldering operations due to their melting temperature. Moreover, these alloys enable an economically attractive couple due to their low cost as compared to other lead-free solders,[8–11] as well as their suitable weldability and low risk of substrate dissolution.[12,13]

The eutectic Sn-0.7 wt.%Cu solder alloy solidified under thermodynamic equilibrium conditions displays microstructures constituted by a Sn-rich matrix and Cu_6Sn_5 intermetallic compounds (IMCs).[14] The eutectic Sn-0.7 wt.%Cu alloy is indicated in the Sn-Cu phase diagram of Fig. 1. According to the phase diagram, two crystalline structures have been observed, η-Cu_6Sn_5 and η'-Cu_6Sn_5, hexagonal and monoclinic, respectively. The allotropic transformation occurs at 186°C, with the η-Cu_6Sn_5 phase being stable above this temperature.[15] Laurila et al.[16] reported that during soldering and subsequent cooling, the time available for conversion to the monoclinic η'-Cu_6Sn_5 phase at low temperatures is not enough. As a consequence, the hexagonal η-Cu_6Sn_5 is maintained as the stable phase. If the temperature is close to 25°C, the transformation does not occur due to kinetic limitations.[17–20]

Mu et al.[21] described that the change from η'-Cu_6Sn_5 to η-Cu_6Sn_5 generates a volumetric expansion that depends on the coefficient of thermal expansion and temperature. This expansion has a deleterious effect on the mechanical properties of the soldered joints.[22,23] Ni additions can decrease the deleterious effects of this allotropic transformation.[15,18]

Selecting a Pb-free solder alloy for microelectronic assembly is based on the comparison of its soldering properties with those of the conventional Sn-Pb alloys.[24] Abtew and Selvaduray[19] cited that the main characteristics for the use of solder alloys are: *liquidus* or eutectic temperatures, wettability, sustainability, solderability, viscosity, density, thermal and electrical properties, corrosion and oxidation behavior, surface tension, reworkability and cost. The properties that provide reliability and performance can be mentioned as coefficient of thermal expansion, elastic modulus, yield strength, shear strength, fatigue and creep behavior of the alloy.

Among all these characteristics, the degree of wetting between the solder alloy and the substrate, which is quantified through contact angle measurements (θ), is the most investigated and reported in the literature.[25–32] Arenas and Acoff[29] and Silva et al.[28] analyzed the wettability of the eutectic Sn-0.7 wt.%Cu alloy on copper (Cu) substrate.

The formed IMC layer due to the contact existing in the alloy/substrate couple is the most important region of the soldering joint, since it is where structural defects nucleate. It is during soldering that the alloy reacts with the substrate causing the formation of a complex IMCs layer. The formation of a soldered joint involves interactions of various and complex metallurgical phenomena, including heat and mass transfer.

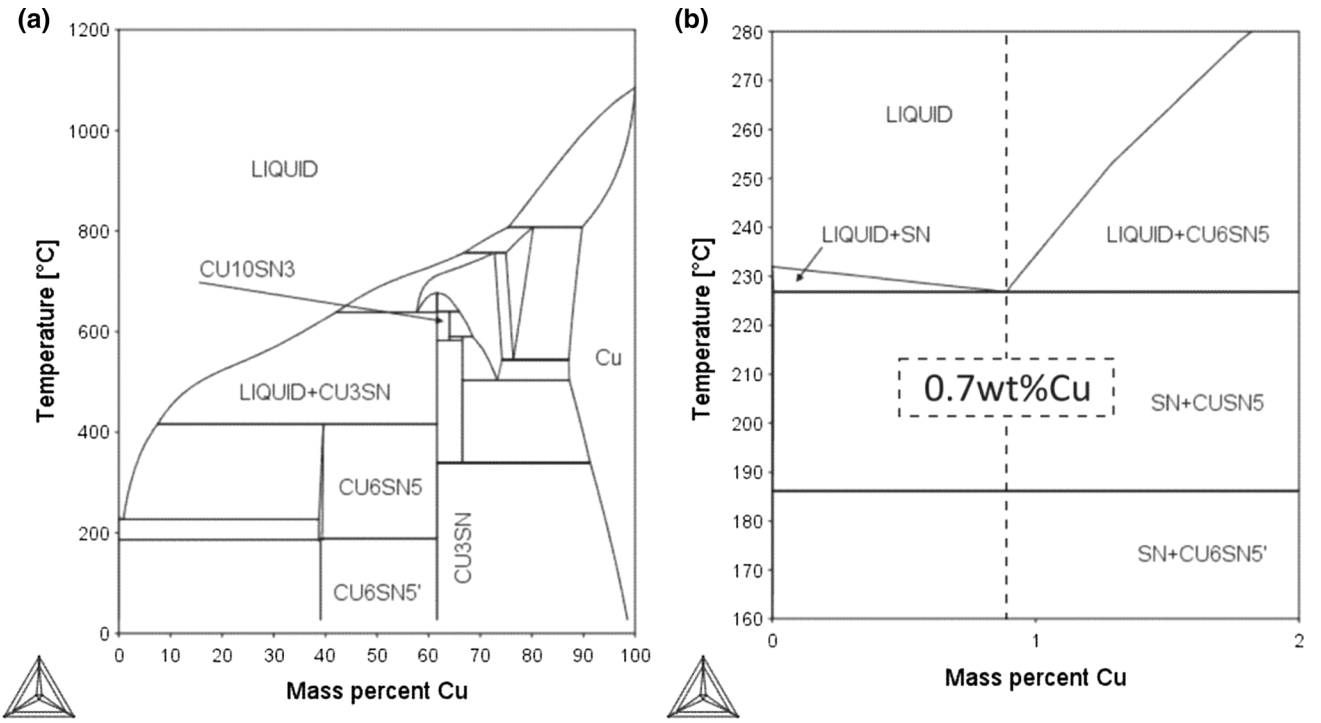

Fig. 1. (a) Sn-Cu phase diagram and (b) details of the eutectic composition computed by the Thermo-Calc software by means of the Solder Demo Database v 1.0.

It is desirable that the layer formed by the IMCs be of small thickness, allowing metallurgical bonds to be achieved. However, a region with excess IMCs may have a deleterious effect on the mechanical strength of the soldered joint. Therefore, degradation by aging in electronic board junctions is a critical concern in the electronic micro-component industry. In order to minimize the problems associated with soldering of electronic microcircuits, the kinetics of interfacial reactions must be understood. These interface reactions depend fundamentally on the movement of atoms by diffusion, which in turn depends on the solidification time.[33] The IMCs (considering type, nature and thickness) formed in interface reactions are preferred regions of degradation of the soldered joints, since IMCs are generally fragile and accumulate many structural defects. Therefore, knowledge about the interactions between solder alloy and substrate, and their effects on the interface reaction become essential for understanding the formation of high-quality soldering joints applied in the electronics industry. Another common phenomenon in the solder alloy/substrate interaction is the surface dissolution of the substrate, when in contact with the molten solder alloy. Alloying elements of the substrate can change the solder alloy chemical composition, forming unforeseen phases.

The substrate plays a key role on the quality of soldered joints in electronics components. The main substrates used are gold (Au), platinum (Pt), palladium (Pd), nickel (Ni), Fe-42% Ni (INVAR) and especially copper (Cu). Other work pieces deserve attention, such as electroless plated substrates obtained from Electroless Nickel/Immersion Gold (ENIG) and Electroless Nickel/Electroless Palladium/Immersion Gold (ENEPIG) processes.[11,34,35] In order to form a proper metallurgical bond between solder alloy and substrate, wetting must take place. This means that a specific interaction must occur between the molten solder alloy and the solid surface of the parts to be joined. The ability of the molten solder to flow or spread during the soldering process is of prime importance for the formation of a proper metallic bond. The term wetting is often used when discussing soldering processes. By definition, wetting is a measure of the ability of a material, generally a liquid, to spread over another material, usually a solid.[19] It is worth noting that the heat transfer efficiency between metal and substrate can be affected by the level of wettability between the two parts. In turn, the heat flux through the solder alloy/substrate interface contributes directly on the evolution of solidification, i.e., it affects the final microstructure of the soldered joints.[28,36]

Several mechanisms of heat transfer occur at the solder/substrate interface, which are generally represented by a transient heat transfer coefficient, h. When a molten solder and substrate surfaces are brought into contact, an imperfect junction is formed. Silva et al.[28] reported that this junction is mainly dependent upon the thermophysical properties of the contacting materials, the roughness of the substrate contacting surface, the melt superheat, the freezing range and wetting behavior. Thus, the heat transfer efficiency, rendered by h, is a key parameter in the control of the solidification kinetics, as it strongly influences the microstructure evolution. A recent investigation[28] demonstrated a decrease in contact angle with increase in the aforementioned transient heat transfer coefficient for eutectic Sn-0.7 wt.%Cu-(xNi) alloys solidified against copper.

The present study aims to investigate the interrelations between the wettability (from wetting angles values), the reaction layer at the solder alloy/substrate interface and results of simulations obtained by a finite difference solidification heat flow program. The results concern the eutectic Sn-0.7 wt.%Cu alloy solidified against three substrates: low carbon steel, copper (Cu) and nickel (Ni). Mechanisms of Newtonian heat transfer (represented by a transient heat transfer coefficient-h) occurring at each solder/substrate couple will be discussed, besides the microstructural characteristics, nature and defects of the IMCs occurring within the reaction layer.

EXPERIMENTAL PROCEDURE

Solidification Experiments

Eutectic Sn-0.7 wt.%Cu castings were produced using commercially pure tin and copper (Table I). The elements were melted inside a SiC crucible in a muffle furnace, homogenized and poured into a stainless-steel split mold. This type of mold allows a change in the bottom part in order not only to close the mold but also to modify the type of alloy/substrate couple. After natural solidification within the mold, each alloy was remelted in situ by radial electrical wiring positioned around a split stainless-steel mold, as can be seen in the solidification apparatus at the top left corner in Fig. 2. Then, when the melt temperature is about 10% above the eutectic temperature (T_E = 227°C), the electric heaters are disconnected and at the same time the water flow at the bottom of the container is started, which allows the onset of directional solidification. The evolution of temperatures along the length of the casting was monitored by fine type J thermocouples (0.2 mm diameter wire). The thermocouples were horizontally placed in line from the bottom towards the top of the casting. So, various relative positions along its length could be monitored with reference to the metal/mold interface. The thermocouples' tips were located in the geometrical center with respect to each circular cross section along the cylindrical mold cavity.

The alloy composition was checked for different positions along the length of the casting. For 1 mm from the water-cooled surface the chemistry was

Table I. Chemical composition (wt.%) of the metals used to prepare the Sn-0.7 wt.%Cu alloy

Metal	Pb	Fe	Sb	Cd	Ni	Ag	Sn
Sn	0.001	0.0025	0.0028	0.0002	0.0001	0.0002	Balance
Cu	–	–	–	–	0.008	–	0.009

Metal	Bi	Zn	Mn	As	Al	Cu
Sn	0.0084	0.0002	–	0.0129	0.0006	0.0004
Cu	–	–	0.008	–	–	Balance

0.77 wt.% Cu, shifting to 0.70 wt.% for a section examined at 32 mm and resulting in 0.68 wt.% for 118 mm. This demonstrated that the alloy composition was very close to the nominal one.

The solidification setup used in the present experiments is shown in Fig. 2. It allows unidirectional extraction of heat through a water-cooled bottom part, which is interchangeable and can be made of two different materials: copper and nickel. Both of them are of interest as electronic soldering substrates. Also, low carbon steel (SAE 1020) material was employed, which is commonly used for mold manufacturing. In the present study it is used for comparison with the other substrates. The surfaces of the bottom-part mold, having 3 mm thickness for each of the tested couples, have been finished with a 1200 grit SiC abrasive paper. A stainless steel split mold was used having an internal diameter of 60 mm, a height of 157 mm and a wall thickness of 5 mm. The amount of alloy prepared to be poured into the mold was sufficient to completely fill it. The lateral inner mold surface was covered with a layer of insulating mass silica-alumina ceramic to minimize radial heat losses and facilitate the removal of the castings. Additional information on specific details of the directional solidification procedure can be found in previous studies.[37–39]

Microstructural Characterization

Samples from the alloy/substrate interface region (bottom right corner image in Fig. 2) were extracted in order to perform Energy Dispersive Spectroscopy x-ray (EDS), x-ray diffraction (XRD) analyzes and microstructural examination. Metallographic preparation consists of mechanical polishing using abrasive papers of subsequent 100, 220, 320, 400, 600, 800 and 1200 meshes and then finishing with 6 μm, 3 μm, 1 μm and 1/4 μm diamond particle sizes. The samples were etched with a solution of 92% (vol) CH_3OH; 5% (vol) HNO_3; 3% (vol) HCl.

The microstructures were observed using an Inspect F50 (FEI) Scanning Electron Microscope (SEM) and an Oxford-XMax energy dispersive x-ray spectrometer was used to characterize the phases formed due to the metallurgical interactions of the alloy with the different substrates: copper, nickel and 1020 steel.

The phases at the alloy/substrate interface region were determined through XRD analyzes performed on the Panalytical x-ray diffractometer, X'pert PRO MRD XL model with PIXcel detector and Cu-Kα target x-ray tubes with Ni filter and radiation with wavelength equal to 1.5604 Å. In the analyzes, a voltage of 45 kV, a current of 40 mA and a scanning interval of $20° \leq 2\theta \leq 90°$ were used.

Wettability Tests

Three substrate's materials were chosen, that is, copper (Cu), nickel (Ni) and 1020 carbon steel. These parts were fabricated from the same materials employed to machine the bottom molds assembling the directional solidification system. As such, comparisons might be possible between the interfaces formed between the alloy and the substrates in both directional solidification and wettability experiments. Triplicate wettability tests were performed for each alloy/substrate couple, which totals nine (9) tests. As such, nine cylindrical samples from the Sn-0.7 wt.%Cu alloy casting were machined having a diameter of 4 mm and height of 4 mm. These specimens were extracted from the directionally solidified (DS) part as can be seen in the bottom left corner of Fig. 2.

A goniometer, Krüss DSHAT HTM Reetz GmbH model, allowed the measurement of contact angles (θ) for each solder alloy/substrate. A schematic illustration of the method can be seen in Fig. 3. The surfaces of the substrates used in the goniometer tests had the same finishing as that employed during directional solidification, that is #1200 grit paper. This is important to ensure greater reliability in the correlation between the parameters obtained through the wettability test and the interfacial heat transfer coefficient, h.

The equipment is able to follow continuously the form of the droplet, which is expressed by contact angles. To avoid oxidation on the alloys samples and on the substrates during the wettability tests, free oxygen in the furnace chamber must be eliminated. This was achieved by injection of Argon into the furnace chamber to create an inert (passive) atmosphere. For each experiment, constant heating rate of 10 K/min, a steady temperature stage at 300°C for 20 min and a natural cooling rate inside the

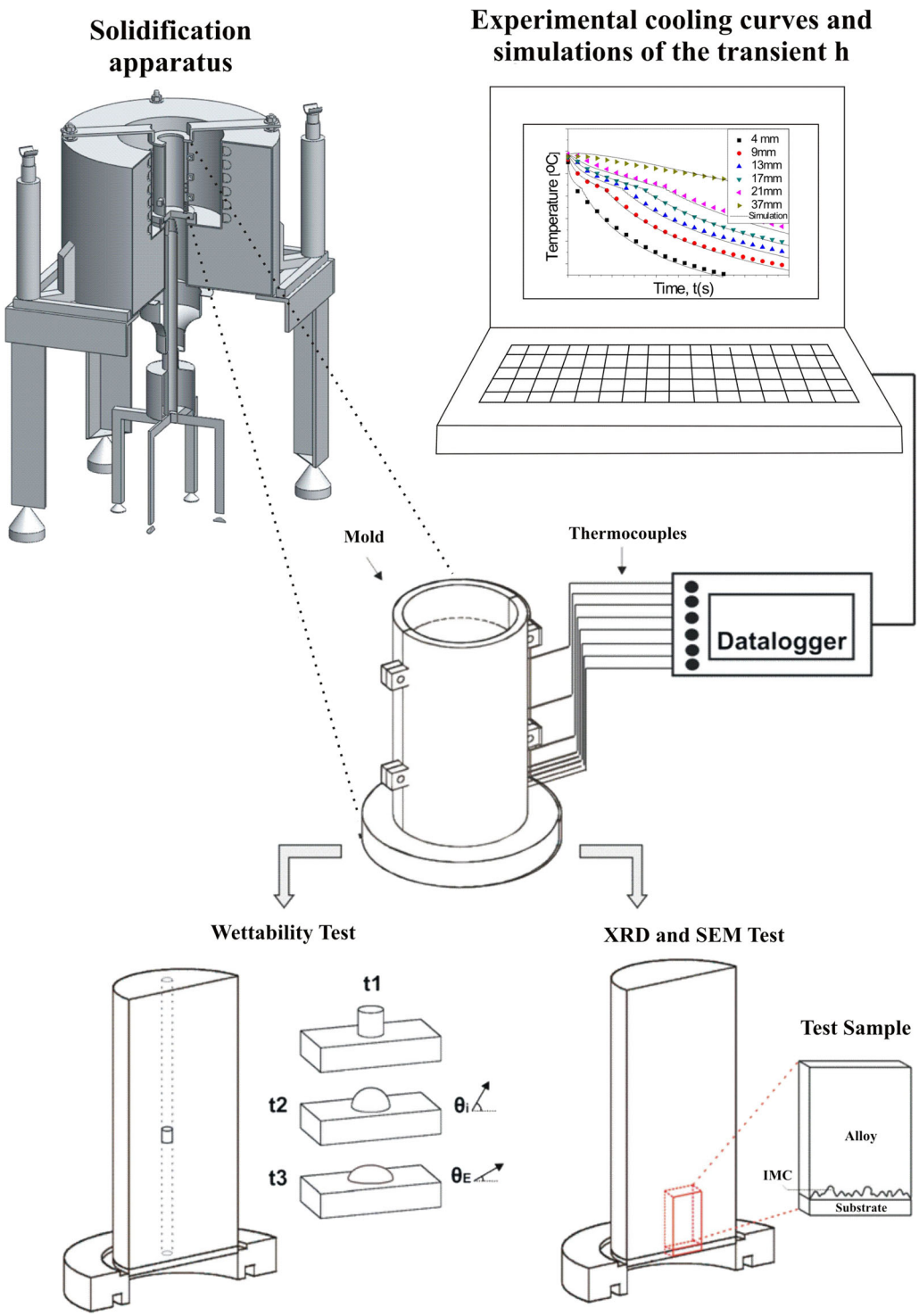

Fig. 2. Sketch of the methods used in this investigation, which are transient solidification to produce the alloy, mathematical modelling to simulate the cooling curves and compute the solder/substrate heat transfer coefficient (h_i), wettability test, x-ray diffraction (XRD) and scanning electron microscope (SEM) analysis.

furnace were carried out. Two different periods of the experimental scatter will be considered: initial stage referred θ_I; and ending stage of the curves when an equilibrium regime is achieved referred θ_e.

MODELLING THE INTERFACE THERMAL CONTACT

Surface wetting is one of the main properties of the solder when molten, becoming a qualifying

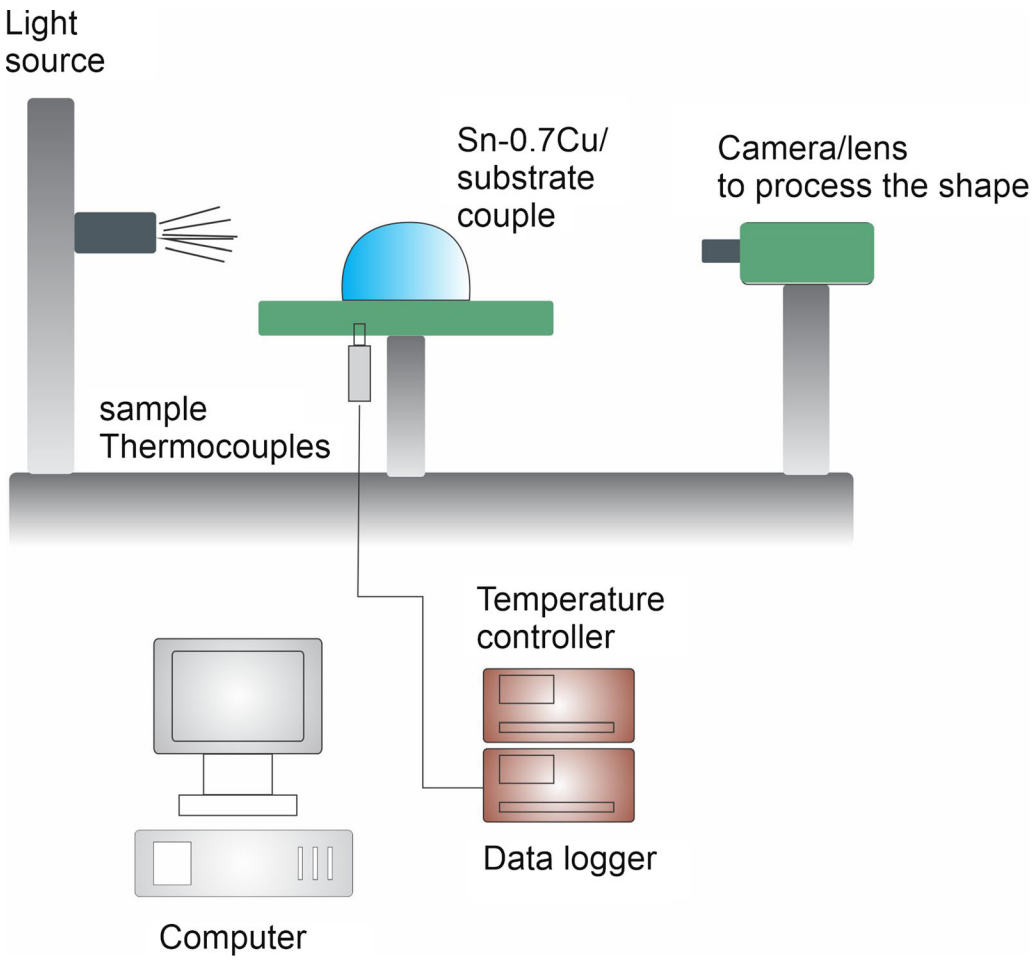

Fig. 3. Sketch of the experimental method applied for the wettability tests.

parameter in the selection of alloys for the interconnection of electronic components into a substrate. Copper and nickel are reported as common substrates used for electronic soldering applications[40] and the wettability behavior of an alloy may considerably differ from one substrate to another. The wettability has been associated with a power function of time (t), $h = at^{-m}$, with (a) and (m) being constants, as described by the heat transfer at metal/mold interfaces of chilled molds.[27,41,42] The ability of heat extraction of a water-cooled mold from the molten metal has an alike aspect with the wettability, since both are affected by the roughness of the mold (substrate), gas entrapment and formation of IMCs at the alloy/substrate interface region. Besides h being an alternative method to evaluate wettability of an alloy over a substrate, replacing the use of the goniometer for the sessile tests, such a casting system is able to provide cooling rates that are similar to that used during reflow procedures in industrial soldering practice.[43] In addition, thermal instrumentation based on contact, such as thermocouples, is not feasible in the reduced soldering joint since they interfere in the thermal history. On the other hand, the inherent larger amount of molten metal within the mold is not sensible to the aforementioned sensing.

In heat transfer problems, the interface boundary condition Eq. 1 is applied in composite walls, i.e., in the case of the present study, air gap interleaved with contact regions between metal and mold. Additionally, there is appreciable temperature drop across the metal/mold interface (Fig. 4), causing a local thermal discontinuity.

$$-k\frac{\partial T}{\partial x}\bigg|_{\text{mold}} = h(T_{\text{M}} - T_{\text{m}}), \tag{1}$$

where T_{M} = molten alloy temperature at the interface; T_{m} = mold surface temperature.

Considering water cooled molds, an overall heat transfer coefficient, h_{ov}, is applied to include the influence of thermal resistances due to air gap, cooling fluid and thickness of the mold wall (Fig. 4):

$$\frac{1}{h_{\text{ov}}} = \frac{1}{h} + \frac{e}{k_{\text{M}}} + \frac{1}{h_{\text{w}}}, \tag{2}$$

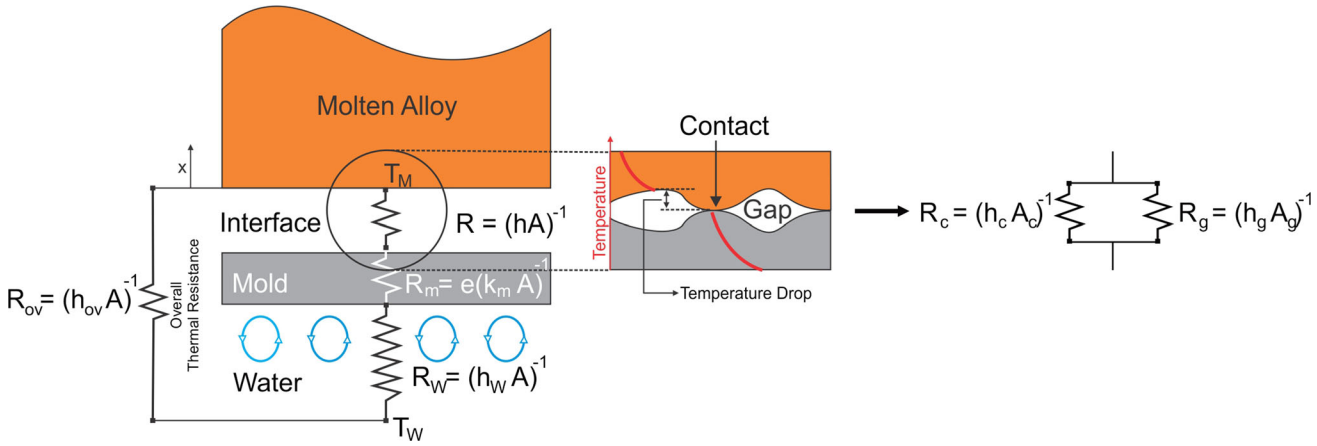

Fig. 4. General scheme of the modeled thermal resistances in a chill mold.

where e = mold thickness (m), k_M = mold thermal conductivity (W m^{-1}K^{-1}); h_W = mold/cooling fluid heat transfer coefficient (W m^{-2}K^{-1})

Since the thermal resistances of mold and cooling fluid are much lower than the one associated with the air gap (that is of about 84% of $1/h_{ov}$), it can be considered that h_{ov} follows the h power law behavior.[44] In addition, the thermal resistance of the cooling fluid can be neglected due to the high value of h_w provided by a turbulent regime. Therefore, isolating h from Eq. 2:

$$h = \frac{k_M \cdot h_{ov}}{k_M - e \cdot h_{ov}}. \tag{3}$$

The thermal contact resistance at the interface, $(A \cdot h)^{-1}$, is composed of two parallel resistances: one due to contact spots $(A_c \cdot h_c)^{-1}$ and other due to the air gaps $(A_g \cdot h_g)^{-1}$ (Fig. 4). Therefore, the heat transfer at the interface is due to thermal conduction across the contact areas from the spots and to the conduction and radiation across the gaps.

$$\frac{1}{hA} = \frac{1}{h_c A_c} + \frac{1}{h_g A_g}, \tag{4}$$

where A = area; subscripts c and g refer to contact spots and gap, respectively.

Besides the interfacial boundary condition, the remaining modeled volume of the molten alloy is based on the heat equation derived from Fourier's law and conservation of energy[45]:

$$\rho \cdot c \cdot \frac{\partial T}{\partial t} = \frac{\partial}{\partial x}\left(k(x) \cdot \frac{\partial T}{\partial x}\right), \tag{5}$$

where k = thermal conductivity [W m^{-1}K^{-1}], q = density [kg m^{-3}], T = temperature [K], c = specific heat [J kg^{-1} K^{-1}]. The thermophysical properties used in the numerical simulations can be found elsewhere.[6]

The latent heat release during solidification at the eutectic temperature is given by a temperature accumulation factor, λ[46]:

$$\lambda = \frac{L}{c}, \tag{6}$$

where L = latent heat [J kg^{-1}]

Equation 5 is numerically solved basing on the Finite Difference method in explicit scheme:

$$(\rho \cdot c)_i \cdot \frac{T_i^{n+1} - T_i^n}{\Delta t} = \frac{1}{\Delta x}\left(k_{i+1} \cdot \frac{T_{i+1}^n - T_i^n}{\Delta x} - k_{i-1} \cdot \frac{T_{i-1}^n - T_i^n}{\Delta x}\right), \tag{7}$$

where n and $n + 1$ refer to temperatures before and after the incremental time interval Δt; i is the position in the mesh according to x axes.

The determination of h_{ov}, is based on a solution method of the inverse heat conduction problem, which takes into account the minimization of the differences among the theoretical temperatures,[47] provided by the aforementioned numerical model (T_{th}), and experimental temperatures (T_{exp}) acquired from thermocouples positioned along the DS casting. The function to be minimized is given by Eq. 8, which accumulates the discrepancies between (T_{th}) and (T_{exp}) from the beginning of the solidification process up to a desired period (n):

$$F = \sum_{time=0}^{n} \left(T_{th} - T_{exp}\right)^2. \tag{8}$$

RESULTS AND DISCUSSION

Thermal Interface Analysis

The heat transfer during the solidification process is directly related not only to the heat extraction efficiency by the substrate but also to the heat transfer coefficient at the interface (h). The cooling curves of the solidified alloy against steel, copper and nickel substrates showed that the Ni substrate was more efficient, allowing the extraction of a greater amount of heat over time (Fig. 5). It is worth noting that the three samples were solidified under

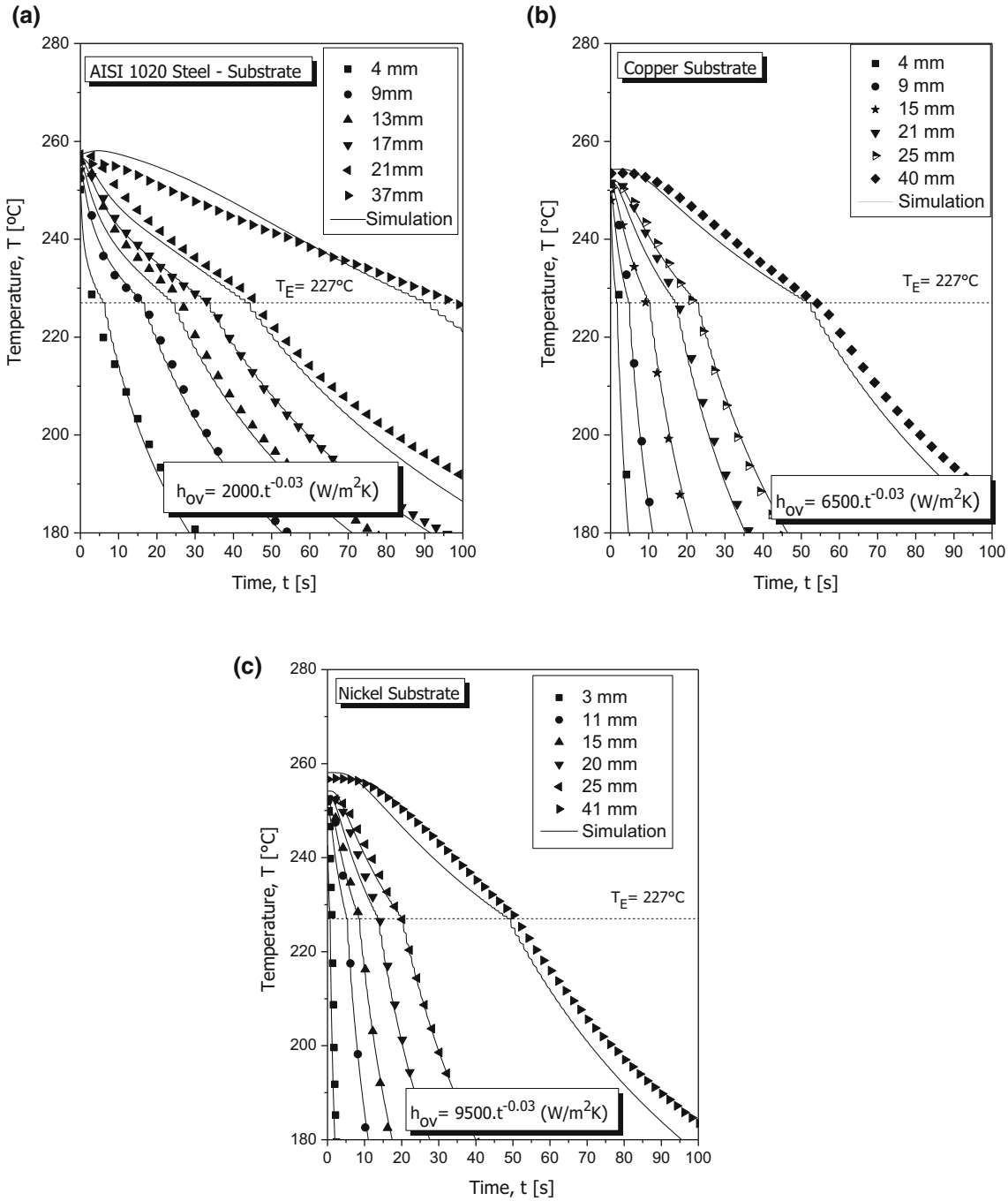

Fig. 5. Experimental cooling curves and numerical simulations used for determining the transient h_{ov} profiles for the substrates (a) AISI 1020 steel; (b) copper; (c) nickel. Positions shown in mm refer to thermocouples' locations from metal/mold interface.

the same experimental conditions just having as difference, the material of the substrates. The solution of the inverse heat conduction problem based on the minimization of the discrepancy between theoretical and experimental thermal profiles allowed the determination of the overall heat transfer coefficients (h_{ov}). They were given by $h_{ov} = 2000t^{-0.03}$, $h_{ov} = 6500t^{-0.03}$ and $h_{ov} = 9500\ t^{-0.03}$ for steel, copper and nickel substrates, respectively, where h_{ov} [W m^{-2}K^{-1}] and t [s]. It is curious to observe that the Ni substrate is associated with a higher heat transfer rate than the other substrates, although it was expected that the Cu substrate would configure this characteristic, since copper has a thermal conductivity 6 × greater than that of Ni and 7 × higher than that of AISI 1020 steel.[48]

Considering the thermal conductivities of copper, nickel and steel as respectively 385 W m^{-1}K^{-1}, 60.7 W m^{-1}K^{-1} and 25.3 W m^{-1}K^{-1},[48] and mold thickness of 3 mm, the time dependent h profiles

(Eq. 3) are shown in Fig. 6a. Analyzes at the alloy/substrate interface region were performed using the SEM line scanning technique and the tool "Stored Vector Profile" of the Zeiss SEM software. Two paths at the interface with the copper substrate show the depth profiles of voids in Fig. 6c and d. The existence of voids (term A_g of Eq. 4) and the consequent reduction in contact between the copper substrate and the alloy (decrease in the A_c term of Eq. 4) justify the loss of the heat transfer efficiency through the interface. For the case of the nickel substrate (Fig. 6b), voids were not found, even when a high magnification was used, which permitted the visualization of the IMCs. Interface analysis was not performed for the experiment against the steel substrate. This is because after the solidification process the sample was found self-detached from the steel substrate indicating the inexistence of any bonding or metallurgical interaction between their surfaces.

The values of h for copper and nickel at the first 10 s can be considered representative for soldering processes, since rapid solidification evolves in this process. With respect to the determined h values, it

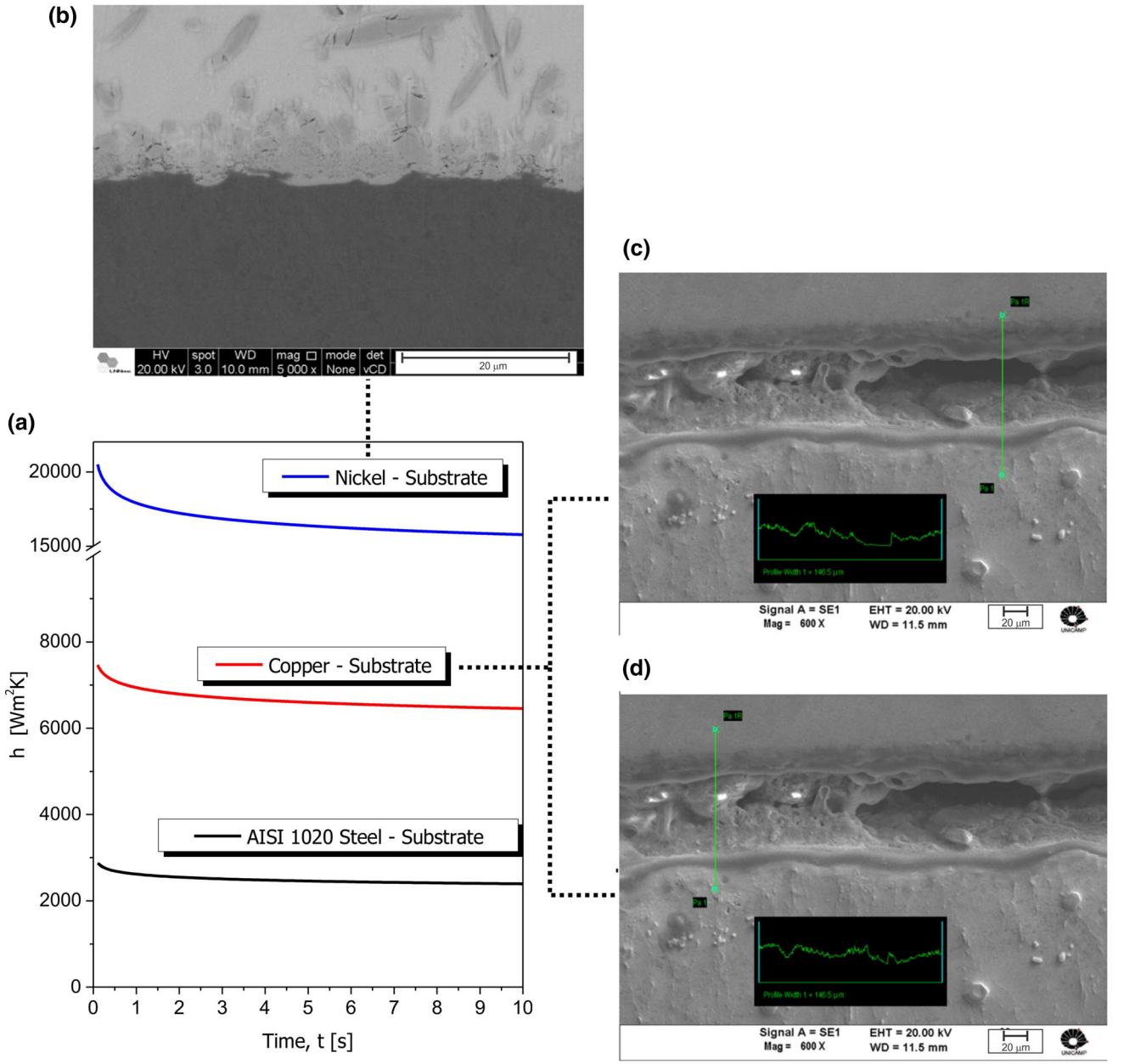

Fig. 6. Relationship between the h profiles and the interaction behavior of the alloy with the substrates (a) Comparative profiles of h for the substrates of nickel, copper and steel; (b) Sn-0.7 wt.%Cu alloy/Ni substrate interface; (c) Sn-0.7 wt.%Cu alloy/Cu substrate interface with line scan analysis (green line) aiming the void region; and (d) Sn-0.7 wt.%Cu alloy/Cu substrate interface with line scan analysis in a more homogeneous region (Color figure online).

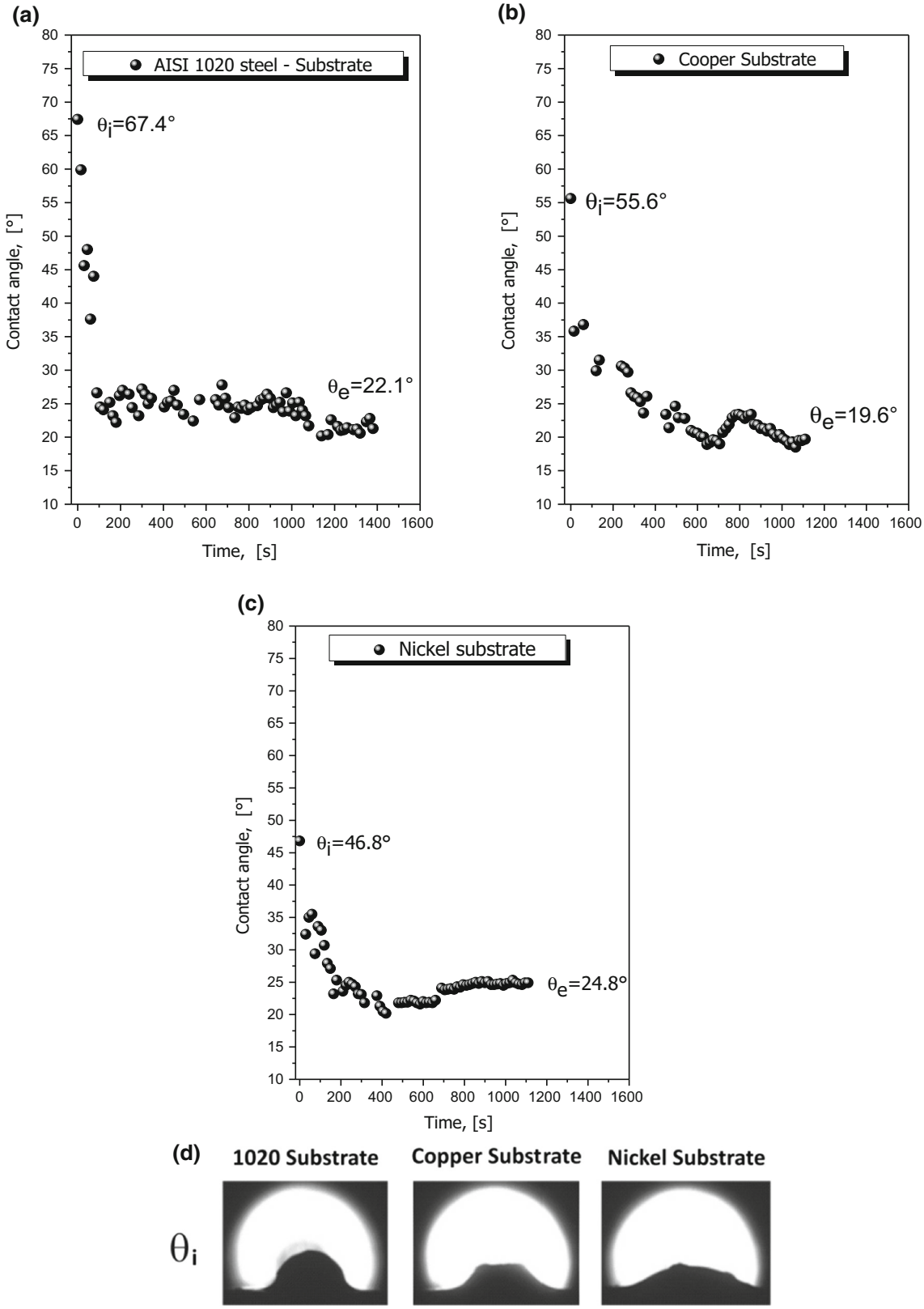

Fig. 7. Representative evolutions of contact angles between molten Sn-0.7 wt.%Cu alloy considering the following surfaces: (a) steel; (b) copper and (c) nickel. (d) Typical optical images during the wetting processes in different substrates.

can be said that they are high due to the existence of bonding forces between the alloy and the substrates surfaces. For example, considering the case of the continuous casting of steel, the overall heat transfer coefficient at the cooled copper mold is around 2000 W $m^{-2}K^{-1}$,[49] which is much lower than the values of the determined h profile for copper in the present investigation (Fig. 6a), since the adhesion between the surfaces of steel billet and mold are avoided in the such industrial process. The cracks observed in the intermetallic particles are due to the polishing process during metallographic preparation of the sample. They were not thermally-driven. The explanation of the dynamics of formation of these voids will be outlined in the next sections, along with the analysis of the formation of IMCs for each of the tested alloy/substrate couples.

Wettability

The plots in Fig. 7 demonstrate the experimental variations of the contact angles between the alloy and the substrate along all the wettability experiments. The results related to the three examined substrate's materials can be seen in Fig. 7. The initial contact angles, θ_i, are inserted to assist a comparison between the tested conditions. This is essential since the changes on the alloy/substrate interaction at the first wetting stages might be directly correlated with heat transfer efficiency between solder and substrate. The initial contact angles of the molten material are considered of prime importance for solidification. This was the subject of a research by Muojekwu et al.[50] They affirmed that the solidified shell formed at the early stages of solidification of a metal depends both on the wetting of the chill by the liquid metal at the initial contact and on the related shrinkage accompanying solidification. These authors found that the peak heat-transfer coefficient (h) concurs with the onset of solidification, when the melt surface temperature is very close to the eutectic temperature. At the next stage, once the solidifying shell becomes self-supporting and a gap is established between the alloy and the chill, the h value tends to decrease intensely. Moreover, the control of the as-solidified microstructure was demonstrated to be connected with the early stages of solidification. For this purpose, the secondary dendrite arm spacing (SDAS) could be expressed as a direct function of h of early stages. This is why in the present research work more emphasis is given to the initial contact angles, instead of the equilibrium ones.

The initial contact angles measured for the Sn-0.7 wt.%Cu in steel, copper and nickel are 67.4°, 55.6° and 46.8°, respectively. In contrast, the degree of the wetting of the couples under equilibrium (θ_e) regime of contact can be considered roughly the same. It is also clear that the extent of wetting attains certain steadiness after about 300 s if considering all examined tests.

It is worth noting that the level of wetting of the couples tested here ensures that affinity between alloy and substrate was achieved since contact angles lower than 90° are always observed. The alloy/steel couple showed the highest contact angle of the three examined couples at the first stages, which allows affirming that this couple represents the lowest wettability. Following the same reasoning, the highest wettability behavior among the three analyzed couples is that of the alloy/nickel one. It is well known that the solder/substrate heat transfer coefficient (h) and the wetting of the couple may sustain a strong correlation between each other. In other words, the higher the heat transfer efficiency between contact points of solder/substrate system, the lower will be θ_I.

In the present study, expressions of the form $h = a(t)^{-0.03}$ have been generated by the mathematical model to represent the heat transfer efficiency of the Sn-0.7 wt.%Cu alloy in all examined conditions. The multipliers 'a' in steel, copper and nickel are 2000, 6500 and 9500, respectively, as can be seen in Table II. These multipliers are well accepted as being related to the wettability of the liquid layer in contact with the substrate surface.[6,27,28] As demonstrated in Table II, a direct correlation may be established between h ('a' values) and θ_I.

Reaction Layer

The produced reaction layers at the interface between the alloy and the substrates were examined in order to comprehend their features. Also, the integrity and nature of the interfaces might be known to permit a more sound analysis regarding the heat transfer efficiency. In the case of the alloy/steel couple, the formation of a reaction layer was totally suppressed. As such, Fig. 8 shows the Sn-Cu/Cu and Sn-Cu/Ni couples SEM microstructures obtained at the joint after the directional solidification process. With regard to the IMCs layers, several energy dispersive spectroscopy (EDS) analyses were performed, in order to better evaluate the elements distributed throughout the interfaces. Some of them are demonstrated in Fig. 8.

It can be noticed that the IMC composition within the IMC layer of the Sn-0.7 wt.%Cu alloy/copper seems to be that of the Cu_6Sn_5 (#point 3 in Fig. 8a), although the results show a higher Sn-content than expected. This result can be explained due to the preferential attack of the Sn-rich phase during chemical etching used to reveal the microstructure. Under such conditions, the EDS analysis probably highlighted even more the Sn presence at the IMC layer. It is also possible to identify the Cu_3Sn (#point 2 in Fig. 8a) as cited by other authors.[51] These features suggest that a transitional region created by diffusion from Cu towards the Cu_6Sn_5-IMC layer has happened. That is why the Cu_3Sn layer is so thin, with thickness of around 0.85 μm on average. Both phases constituting the IMC interface

Table II. Wetting angles and *h* constants typified by the multipliers '*a*' determined for the for Sn-0.7 wt.%Cu solder alloy on various substrate surfaces

Substrates	Average θ_i—initial (first 45 s)	"*a*"
AISI 1020 Steel	47.7 ± 8.1	2000
Copper	42.7 ± 8.6	6500
Nickel	38.1 ± 5.8	9500

for the alloy/copper couple are confirmed by XRD analysis in Fig. 9.

A $(Cu,Ni)_6Sn_5$ IMC layer characterizes the Sn-Cu alloy/nickel couple as shown in Fig. 8b. The at.% contents of Ni and Cu agree with those reported in other investigations typifying such IMC.[52] The SEM–EDS #point 3 data in Fig. 8b reveals some presence of Ni inside the alloy. It appears that this is due to the dissolution of Ni in the molten alloy during solidification of the Sn-0.7 wt.% Cu alloy against the nickel mold. Despite no detection in the SEM–EDS analysis, Ni_3Sn_4 phase has been indexed by utilizing XRD results as can be seen in Fig. 9b. Typical dendritic microstructures of the alloy are shown in Fig. 8a and b considering transversal and longitudinal views with respect to the heat flux direction.

Dissolution of Ni or Cu to the molten Sn-Cu alloy was verified for both tested couples during directional solidification. The chemical interaction ahead of the interface is a result of the strong diffusion of Cu and Ni from the substrates towards the molten alloy as explained by Laurila et al.[53] Another important aspect is that the alloy solidification against the Ni mold suppresses the growth of the Cu_3Sn IMC layer within the reaction interface. This is in agreement with previous results by various authors,[15,21,53] who stated that the presence of Ni in the Sn-0.7 wt.%Cu molten alloy inhibits the formation of the Cu_3Sn IMC. Other than, in the case of the alloy/nickel couple, less content of copper is available. As such, the Cu-rich Cu_3Sn IMC formation is prevented simply due to the non-disposal of copper along with the reaction.

Each IMC layer is characterized by its own thermophysical properties, which, in turn, diverge from those of the pure elements. For example, the thermal conductivities of the Cu_3Sn and Cu_6Sn_5 phases are 69.8 W $m^{-1}K^{-1}$ and 34.2 W $m^{-1}K^{-1}$ respectively.[54] This means that each produced layer between the alloy and the substrate may operate as barriers to heat extraction. The thermal conductivity, in association with the thickness of each phase, affects the total thermal resistance at the interface and, as a consequence, the heat flow during cooling.

The absence of a layer formed above the carbon steel surface resulted in lack of contact, i.e., higher presence of imperfections and voids are expected to occur. Under such configuration, heat passage is minimized. The double $Cu_3Sn + Cu_6Sn_5$ layer allows stronger adhesion between the alloy and the copper substrate. However, when temperature achieves 186°C during the cooling stage, an allotropic transformation from the high temperature hexagonal η-Cu_6Sn_5 phase to the low temperature monoclinic η'-Cu_6Sn_5 phase happens. This transformation results in volume shrinkage.[21] Hence, small imperfections and voids tend to be produced at the Cu_3Sn/Cu_6Sn_5 and Cu_6Sn_5/Sn-Cu alloy boundaries (Fig. 10). These features counteract the high thermal conductivity of copper, so that heat flow decreased.

Fig. 8. Typical microstructures of the alloy for transversal and longitudinal views and compositions of the IMC layers as well the surrounding areas in both (a) the Sn-0.7 wt.%Cu alloy/copper and (b) the Sn-0.7 wt.%Cu alloy/nickel couples obtained after directional solidification experiments. ▶

The addition of Ni decreases the undesirable thermal contraction by stabilizing the hexagonal Cu_6Sn_5 IMC at temperatures below 186°C. In addition, Cu atoms within the IMC may be replaced with Ni atoms due to the mutual solubility, and so forming the $(Cu,Ni)_6Sn_5$ IMC. The high stability of the $(Cu,Ni)_6Sn_5$ IMC layer guarantee a better contact between the Sn-Cu alloy and the nickel substrate.[34] This explains the higher heat transfer efficiency (i.e., higher h) associated with this couple as compared to the h values determined to the others examined couples, that is, alloy/steel and alloy/copper.

Given the above, the heat transfer efficiency of the copper substrate is lower than that of the nickel substrate. This is thanks to the occurrence of small voids at the boundaries between the IMC layers and between the IMC layer and the Sn-0.7 wt.%Cu alloy. The existence of voids provokes a reduction in the contact areas between the copper substrate and the alloy. As a consequence, loss of the heat transfer efficiency through the interface is attained.

CONCLUSIONS

- The proposed solution of the inverse heat conduction problem allowed the determination of the overall Sn-0.7 wt.%Cu solder alloy/substrate heat transfer coefficients (h_{ov}), which were shown to be given by:
  Steel substrate: $h_{ov} = 2000t^{-0.03}$.
  Copper substrate $h_{ov} = 6500t^{-0.03}$;
  Nickel substrate $h_{ov} = 9500t^{-0.03}$
  where h_{ov} [W $m^{-2}K^{-1}$] and t [s].
- The wettability tests allowed the experimental variations of the contact angles between the Sn-0.7 wt.%Cu solder alloy and the substrates to be determined. The initial contact angles, θ_i, were given by:
  Steel substrate: $\theta_i = 67.4°$

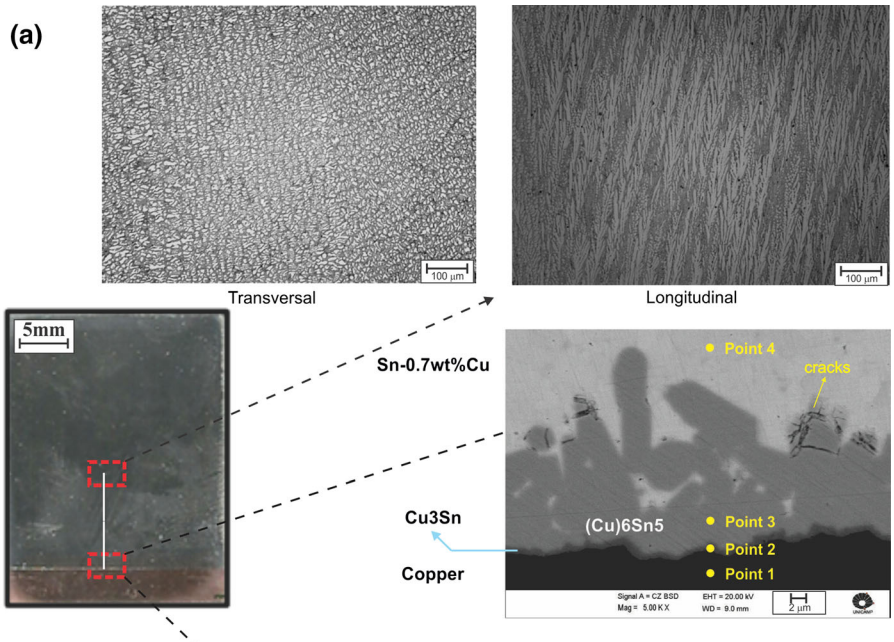

Point (at.%)	Cu	Sn	Total
Point 1	99.67	0.33	100
Point 2	63.42	36.58	100
Point 3	32.16	67.84	100
Point 4	1.20	98.80	100

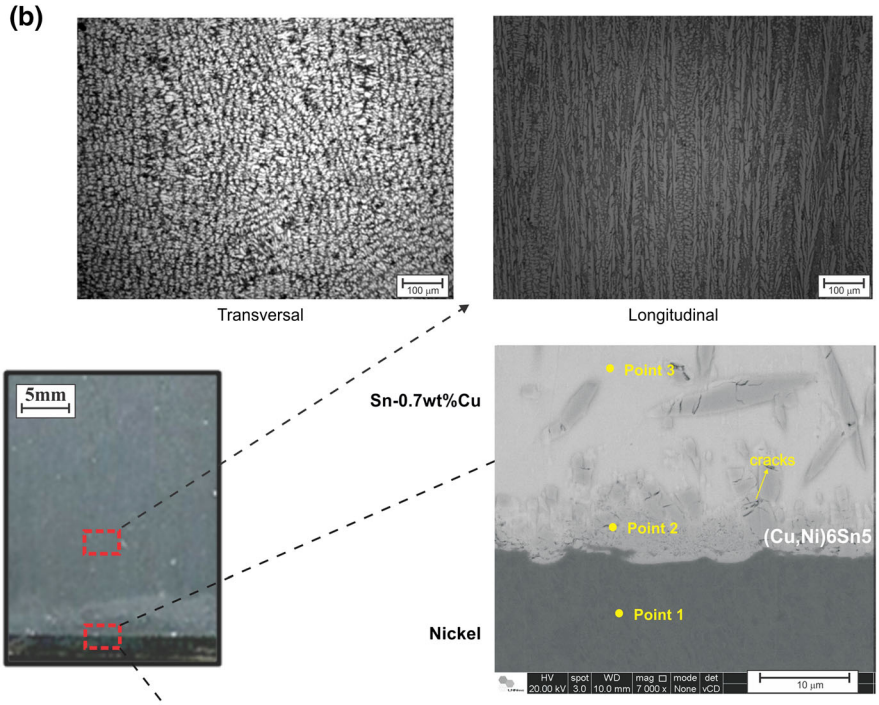

Point (at.%)	Ni	Cu	Sn	Total
Point 1	97.34	0.00	2.66	100
Point 2	14.95	21.26	63.79	100
Point 3	0.45	0.57	98.98	100

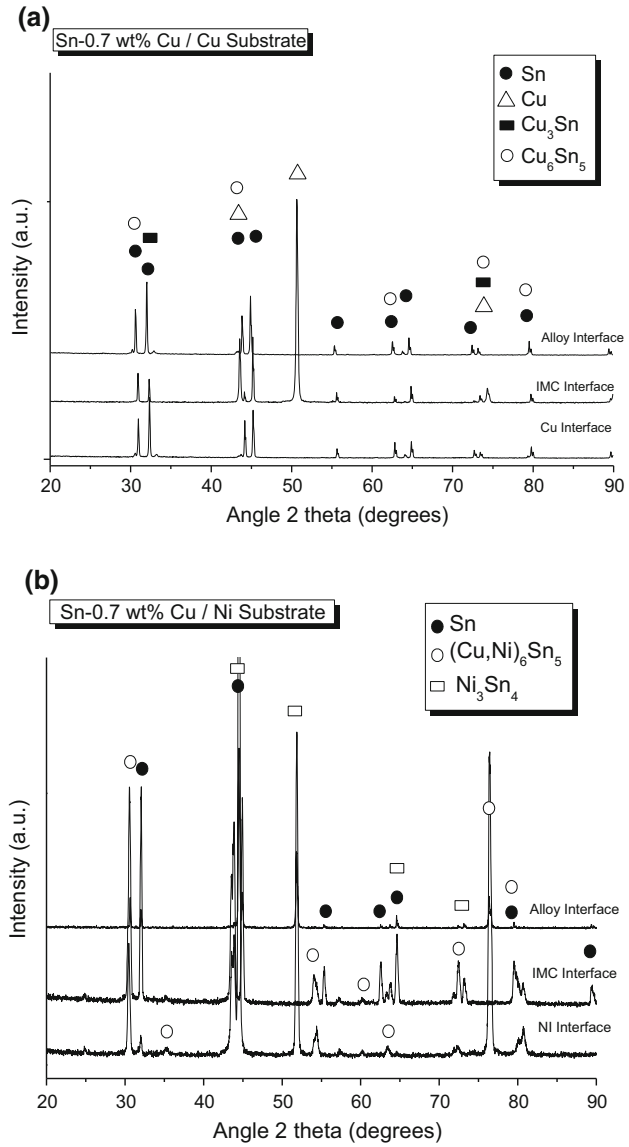

Fig. 9. X-ray diffraction (XRD) patterns for three distinct regions identified across: (a) the Sn-0.7 wt.%Cu alloy/copper and (b) the Sn-0.7 wt.%Cu alloy/nickel couples.

Copper substrate: $\theta_i = 55.6°$
Nickel substrate: $\theta_i = 46.8°$

It can be seen that a direct correlation exists between the multipliers of the $h_{ov} = a(t)^{-0.03}$ equations and θ_i, that is, these multipliers (a) can be regarded as an indicative parameter of the wettability of the liquid layer in contact with the substrate surface.

- The integrity and nature of the solder/substrates interfaces were examined to permit more sound analyses regarding the heat transfer efficiency. In the case of the alloy/steel couple, the formation of a reaction layer was shown to be totally suppressed. The IMC layer of the Sn-0.7 wt.%Cu alloy/copper substrate was shown to be formed by Cu_6Sn_5. A $(Cu,Ni)_6Sn_5$ IMC layer was shown to characterize the Sn-0.7 wt.%Cu alloy alloy/nickel couple.
- Dissolution of Ni or Cu to the molten Sn-Cu alloy was shown to occur for both tested couples during solidification. The addition of Ni was shown to decrease the thermal contraction by stabilizing the hexagonal Cu_6Sn_5 IMC at temperatures below 186°C. Moreover, Cu atoms within the IMC may be replaced with Ni atoms due to the mutual solubility, and so forming the $(Cu,Ni)_6Sn_5$ IMC. The high stability of the $(Cu,Ni)_6Sn_5$ IMC layer guarantee a better contact between the Sn-Cu alloy and the nickel substrate, which explains the higher heat transfer efficiency (i.e., higher h) associated with this couple as compared to the h values determined to the alloy/steel and alloy/copper couples.
- Heat transfer modelling can be a useful tool to predict the bonding quality of the joints, regarding the existence of voids, which reduces the heat transfer efficiency at the metal/substrate interface region.

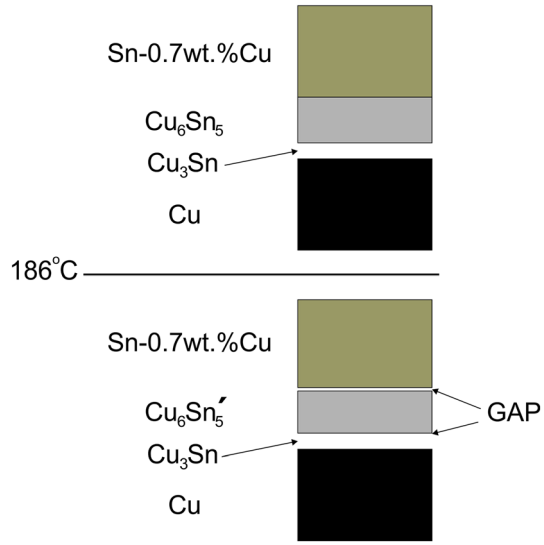

Fig. 10. Schematic representation of gap formation due to the hexagonal-to-monoclinic allotropic transformation of the Cu_6Sn_5 phase along the cooling stage.

ACKNOWLEDGMENTS

The authors are grateful to FAPESP-São Paulo Research Foundation, Brazil (Grants: 2017/16058-9, 2017/15158-0 and 2017/12741-6), Capes-Coordenação de Aperfeiçoamento de Pessoal de Nível Superior, Brazil (Funding Code 001), CNPq-National Council for Scientific and Technological Development (Grant 408576/2016-2) and FAPEAM

(Amazonas State Research Foundation) for their financial support. The authors would like to thank the Brazilian Nanotechnology National Laboratory—LNNano for allowing us to use its facilities.

REFERENCES

1. European Parliament, *Off. J. Eur. Union* 54, 88 (2011).
2. R.A. Islam, Y.C. Chan, W. Jillek, and S. Islam, *Microelectron. J.* 37, 705 (2006).
3. J. Koo, C. Lee, S.J. Hong, K.-S. Kim, and H.M. Lee, *J. Alloys Compd.* 650, 106 (2015).
4. H. Ma and J.C. Suhling, *J. Mater. Sci.* 44, 1141 (2009).
5. B.L. Silva, N. Cheung, A. Garcia, and J.E. Spinelli, *J. Alloys Compd.* 632, 274 (2015).
6. B.L. Silva, N. Cheung, A. Garcia, and J.E. Spinelli, *J. Electron. Mater.* 42, 179 (2013).
7. T. Ventura, S. Terzi, M. Rappaz, and A.K. Dahle, *Acta Mater.* 59, 1651 (2011).
8. I.T.L. Moura, C.L.M. Silva, N. Cheung, P.R. Goulart, A. Garcia, and J.E. Spinelli, *Mater. Chem. Phys.* 132, 203 (2012).
9. C.M. Gourlay, K. Nogita, S.D. McDonald, T. Nishimura, K. Sweatman, and A.K. Dahle, *Scr. Mater.* 54, 1557 (2006).
10. E. Havia, E. Bernhardt, T. Mikkonen, H. Montonen, M. Alatalo, in *ELTUPAK Conference Proceedings* (2005), pp. 1–15.
11. J.-W. Yoon, Y.-H. Lee, D.-G. Kim, H.-B. Kang, S.-J. Suh, C.-W. Yang, C.-B. Lee, J.-M. Jung, C.-S. Yoo, and S.-B. Jung, *J. Alloys Compd.* 381, 151 (2004).
12. A.A. El-Daly and A.E. Hammad, *J. Alloys Compd.* 509, 8554 (2011).
13. E. Çadırlı, U. Böyük, S. Engin, H. Kaya, N. Maraşlı, and A. Ülgen, *J. Alloys Compd.* 486, 199 (2009).
14. S.K. Kang, in *Handbook of Lead-Free Solder Technology for Microelectronic Assemblies*, ed. by K.J. Puttlitz, K.A. Stalter (Marcel Dekker, New York, 2004), pp. 280-300.
15. K. Nogita and T. Nishimura, *Scr. Mater.* 59, 191 (2008).
16. T. Laurila, V. Vuorinen, and J.K. Kivilahti, *Mater. Sci. Eng. R* 49, 1 (2005).
17. K. Nogita, *Intermetallics* 18, 145 (2010).
18. K. Nogita, S.D. McDonald, H. Tsukamoto, J. Read, S. Suenaga, and T. Nishimura, *Trans. Jpn. Inst. Electron. Packag.* 2, 46 (2009).
19. M. Abtew and G. Selvaduray, *Mater. Sci. Eng. R* 27, 95 (2000).
20. D.R. Frear, H.S. Morgan, S.N. Burchett, and J.H. Lau, *The Mechanics of Solder Alloy Interconnects* (New York: Van Nostrand Reinhold, 1994).
21. D. Mu, J. Read, Y. Yang, and K. Nogita, *J. Mater. Res.* 26, 2660 (2011).
22. C. Yu, J. Liu, H. Lu, P. Li, and J. Chen, *Intermetallics* 15, 1471 (2007).
23. H.P.R. Frederikse, R.J. Fields, and A. Feldman, *J. Appl. Phys.* 72, 2879 (1992).
24. L. Zhang, S. Xue, L. Gao, G. Zeng, Z. Sheng, Y. Chen, and S. Yu, *J. Mater. Sci. Mater. Electron.* 20, 685 (2009).
25. M. Dias, T.A. Costa, B.L. Silva, J.E. Spinelli, N. Cheung, and A. Garcia, *Microelectron. Reliab.* 81, 150 (2018).
26. B.L. Silva, F. Bertelli, M.V. Canté, J.E. Spinelli, N. Cheung, and A. Garcia, *J. Mater. Sci. Mater. Electron.* 27, 1994 (2016).
27. W.L.R. Santos, B.L. Silva, F. Bertelli, J.E. Spinelli, N. Cheung, and A. Garcia, *Appl. Therm. Eng.* 107, 431 (2016).
28. B.L. Silva, N. Cheung, A. Garcia, and J.E. Spinelli, *Mater. Lett.* 142, 163 (2015).
29. M.F. Arenas and V.L. Acoff, *J. Electron. Mater.* 33, 1452 (2004).
30. X. Zhang, Z. Yuan, H. Zhao, L. Zang, and J. Li, *Chin. Sci. Bull.* 55, 797 (2010).
31. D.B. Knoor and L.E. Felton, in *Proceedings of the Design and Manufacturing Conference* (ASME, New York, 1994), pp. 27–34.
32. M.J. Rizvi, C. Bailey, Y.C. Chan, and H. Lu, *J. Alloys Compd.* 438, 116 (2007).
33. T.K. Lee, T.R. Bieler, C.U. Kim, and H. Ma, *Fundamentals of Lead-Free Solder Interconnect Technology: From Microstructures to Reliability*, 1st ed. (New York: Springer, 2015).
34. K. Nogita, C.M. Gourlay, and T. Nishimura, *JOM J. Min. Met. Mater. Sci.* 61, 45 (2009).
35. C. Shen, Z. Hai, C. Zhao, J. Zhang, J.L. Evans, M.J. Bozack, and J.C. Suhling, *Materials* 10, 451 (2017).
36. J.E. Spinelli, N. Cheung, P.R. Goulart, J.M.V. Quaresma, and A. Garcia, *Int. J. Therm. Sci.* 51, 145 (2012).
37. R.V. Reyes, T.S. Bello, R. Kakitani, T.A. Costa, A. Garcia, N. Cheung, and J.E. Spinelli, *Mater. Sci. Eng. A* 685, 235 (2017).
38. B.L. Silva, V.C.E. da Silva, A. Garcia, and J.E. Spinelli, *J. Electron. Mater.* 46, 1754 (2017).
39. B. Donadoni, L. Gomes, A. Garcia, J. Spinelli, B.M.C. Donadoni, L.F. Gomes, A. Garcia, and J.E. Spinelli, *Metals* 8, 1 (2018).
40. S. Chen, C. Yang, H. Wu, R.-B. Chang, and C. Hsu, *Mater. Chem. Phys.* 132, 481 (2012).
41. N. Cheung, N.S. Santos, J.M.V. Quaresma, G.S. Dulikravich, and A. Garcia, *Int. J. Heat Mass Transf.* 52, 451 (2009).
42. F. Bertelli, J.D. Faria, P.R. Goulart, C. Brito, N. Cheung, and A. Garcia, *Appl. Therm. Eng.* 96, 454 (2016).
43. J.E. Spinelli, B.L. Silva, and A. Garcia, *Mater. Des.* 58, 482 (2014).
44. J.K. Brimacombe, I.V. Samarasekera, and J.E. Lait, in *Continuous Casting* (Iron and Steel Society of AIME, Warrendale, 1984), pp. 29–104.
45. F.P. Incropera and D.P. Dewitt, *Fundamentals of Heat and Mass Transfer*, 3rd ed. (New York: Wiley, 1990).
46. R.W. Ruddle, *The Solidification of Castings*, 2nd ed. (London: Institute of Metals, 1957).
47. J.V. Beck, B. Blackwell, and C.R. St, *Clair, Inverse Heat Conduction: III—Posed Problems* (New York: Wiley, 1985).
48. MatWeb: Online Materials Information Resource. http://www.matweb.com/ Accessed 5 Jan 2019.
49. N. Cheung, C.A. Santos, J.A. Spim, and A. Garcia, *Appl. Math. Model.* 30, 104 (2006).
50. C.A. Muojekwu, I.V. Samarasekera, and J.K. Brimacombe, Metall. *Mater. Trans.* 26, 361 (1995).
51. S. Lin, T.L. Nguyen, S. Wu, and Y. Wang, *J. Alloys Compd.* 586, 319 (2014).
52. S.A. Belyakov and C.M. Gourlay, *Intermetallics* 25, 48 (2012).
53. T. Laurila, J. Hurtig, V. Vuorinen, and J.K. Kivilahti, *Microelectron. Reliab.* 49, 242 (2009).
54. R.J. Fields, S.R. Low III, and G.K. Lucey Jr., in *Proceedings of the TMS Symposium* (Metal Science of Joining, Cincinnati, 1991), pp. 20–24.